Journal of Molecular Spectroscopy **200,** 253–260 (2000)
doi:10.1006/jmsp.1999.8053, available online at http://www.idealibrary.com on IDEAL®

High-Resolution Study of the BaI $A^2\Pi$ Electronic State

R. F. Gutterres,*,† J. Vergès,* and C. Amiot*,[1]

*Laboratoire Aimé Cotton, Université Paris-Sud, Bât 505, Campus d'Orsay 91405, Orsay Cedex, France; and †Laboratório de Espectroscopia e Laser, Universidade Federal Fluminense, Campus da Boa Viagem, Niterói, RJ 24210-340, Brazil

Received November 2, 1999; in revised form December 10, 1999

Near-infrared and visible spectra of the $A^2\Pi$–$X^2\Sigma^+$, $C^2\Pi_{1/2}$–$A^2\Pi_{1/2}$, $C^2\Pi_{1/2}$–$B^2\Sigma^+$, and $C^2\Pi_{1/2}$–$X^2\Sigma^+$ band systems of the BaI molecule were recorded by using Fourier transform spectroscopy (FTS). The spectra were produced from the chemiluminescent reaction Ba + I_2 and also by using laser-induced fluorescence (LIF) technique in which the laser sources were a Ti:sapphire single-mode laser, a dye single-mode laser, and a Kr^+ multimode ion laser. Resolved rotational data, originating from 19 vibrational levels ($0 \le v \le 5$ and $7 \le v \le 19$) of the $A^2\Pi$ state, 24 vibrational levels ($0 \le v \le 18$ and $20 \le v \le 24$) of the $X^2\Sigma^+$ state, and 8 vibrational levels ($1 \le v \le 2$ and $9 \le v \le 14$) of the $C^2\Pi$ state, were used in the final analysis. Previously recorded data for the $B^2\Sigma^+$–$X^2\Sigma^+$ and $C^2\Pi$–$X^2\Sigma^+$ systems, taken from R. F. Gutterres, J. Vergès, and C. Amiot, *J. Mol. Spectrosc.* **196,** 29–44 (1999) and from C. A. Leach, A. A. Tsekouras, and R. N. Zare, *J. Mol. Spectrosc.* **153,** 59–72 (1992), were added to the present work data field. Accurate and improved molecular constants, for the $X^2\Sigma^+$, $B^2\Sigma^+$, $A^2\Pi$, and $C^2\Pi$ states, were derived from a simultaneous treatment of the whole data set.

Key Words: Fourier transform spectroscopy; laser-induced fluorescence; BaI $A^2\Pi$ electronic state; molecular constants.

I. INTRODUCTION

The alkaline–earth monohalides *MX* (where *M* is the metal and *X* the halogen) have attracted the interest of theoretical and experimental spectroscopists for a long time. These molecules are highly ionic compounds and have nine valence electrons outside closed shells. The structure of the ground electronic state and the structures of the first excited electronic states can be described by an unpaired electron and a molecular ion core consisting of two closed-shell ions M^{2+} and X^-. Theoretically it is expected that the electronic structure of these radicals should have a behavior similar to the one of the alkali atoms. The electronic states $A'\ ^2\Delta$, $A^2\Pi$, $B^2\Sigma^+$, and $C^2\Pi$ would be formed from the excitation of the unpaired *ns* electron to the low-lying $(n-1)$ states. Different ionic bonding models have been developed to represent the structure of these first excited states, e.g., the *electrostatic polarization* model (*3, 4*) and the *ligand-field approach* (*5*). From these models, predictions for both the transition energies and the permanent and transition dipole moments have been done for several alkaline–earth monohalide molecules, including the BaI molecule (*6, 7*).

The first observation of vibrational bands of the BaI $C^2\Pi$–$X^2\Sigma^+$ band system was made in 1928 by Walters and Barratt (*8*). Later, Mesnage (*9*) studied the $C^2\Pi$–$X^2\Sigma^+$ bandheads and more detailed vibrational analyses of this band system were performed by Patel and Shah (*10*) and Rao *et al.* (*11*). In their work, Patel and Shah (*10*) also recognized that the absorption spectrum in the region of 380 nm observed by Walters and Barratt (*8*) was caused by two other electronic band systems: $E^2\Sigma^+$–$X^2\Sigma^+$ at about 374 nm and $D^2\Sigma^+$–$X^2\Sigma^+$ at about 388 nm. Bradford *et al.* (*12*) observed the chemiluminescence reaction Ba + I_2 and determined that the infrared emission was issued from two unobserved electronic transitions: $A^2\Pi$–$X^2\Sigma^+$ and $B^2\Pi$–$X^2\Sigma^+$. In all previously mentioned works the experiments were unable to resolve the individual rotational transitions, which are very closely spaced, mainly because of the fact that the large mass of barium and iodine atoms results in very small rotational constants.

However, since 1981 there has been a high-accuracy systematic study of the $C^2\Pi$–$X^2\Sigma^+$ band system with rotational resolution. The $C^2\Pi$–$X^2\Sigma^+$ (0–0) band has been studied by using population-labeling optical–optical double resonance (PLOODR) at first by Johnson *et al.* (*13*) and after that by Johnson and Zare (*14*). The same band has been studied also by using selectively detected laser-induced fluorescence (SDLIF) by Johnson *et al.* (*15*). In the last three mentioned works a collimated beam of the BaI molecule obtained from an oven source was used and the molecular constants for the $C^2\Pi$ and $X^2\Sigma^+$ states were determined. It must also be emphasized that the molecular constants reported in the last three mentioned works were found to be essentially equal to each other. Nevertheless, using a crossed-beam apparatus, SDLIF, and laser-induced fluorescence (LIF), Zhao *et al.* (*16*) performed a powerful study of the $C^2\Pi$–$X^2\Sigma^+$ (0–0) band in which high-rotational levels (J'' up to nearly 500) were observed. From this data set, and combining with previous results (*13–15*), it was possible for the authors to determine an improved and more general set of molecular constants. Using PLOODR, Leach *et al.* (*17*) observed and assigned the $C^2\Pi$–$X^2\Sigma^+$ (8–8) band. Finally, Leach *et al.* (*2*) performed a general rovibra-

[1] To whom correspondence should be addressed. E-mail: claude.amiot@lac.u-psud.fr.

0022-2852/00 $35.00

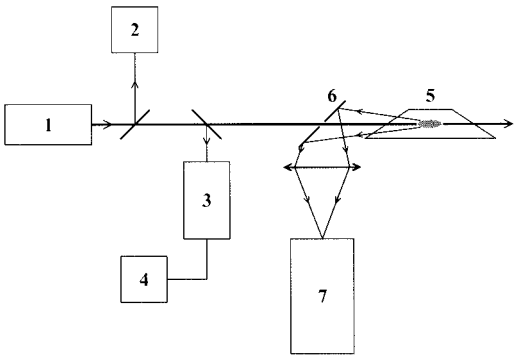

FIG. 1. Scheme of the experimental setup. 1, Laser source (Ti:sapphire or dye single-mode lasers or Kr^+ multimode ion laser). 2, Lambdameter. 3, Fabry–Perot spectrum analyzer. 4, Oscilloscope recording the transmission fringes of the spectrum analyzer. 5, Heat-pipe oven. 6, Pierced mirror collecting the fluorescence light backwards with respect to the laser beam. 7, Two meters optical path length Fourier transform spectrometer. Devices 1, 2, 3, and 4 are not used in the recording of the chemiluminescent spectrum and devices 2, 3, and 4 in the experiment using a Kr^+ laser.

tional analysis of the BaI $C^2\Pi$–$X^2\Sigma^+$ band system with $v \leq 12$. The observed bands ($\Delta v = 0$), with $v = 0$, 1, 4, 8, and 12, were recorded by SDLIF and, in addition, the bands ($\Delta v = 0$), with $v = 0$, 1, 2, and 3, were measured by LIF, in which the undispersed fluorescence was detected. The obtained data were combined with previous results (*15*, *14*, *17*) and also with microwave measurements of low J'' values for $v = 0$–5 of the $X^2\Sigma^+$ state obtained by Töring and Döbl (*18*). A set of 31 molecular constants was calculated from a weighted nonlinear fit; it reproduced the 5032 observed transition wavenumbers with a standard deviation of 2.37×10^{-3} cm^{-1} and the values obtained for these constants by the authors improved the values obtained by Rao *et al.* (*11*).

TABLE 1
Vacuum Wavenumber σ and Emitted Power P of the Used Laser Radiation Sources

Laser	σ (cm^{-1})	P (W)	σ (cm^{-1})	P (W)	σ (cm^{-1})	P (W)
Ti:sapphire	10042.86	0.3	10393.95	0.3	10695.23	0.4
	10056.79	0.2	10394.52	0.4	10726.83	1.0
	10100.22	0.3	10422.82	0.4	10822.36	0.4
	10150.27	0.4	10422.89	0.3	10837.34	1.0
	10200.50	0.4	10436.81	0.4	10869.46	1.1
	10257.79	0.2	10501.80	0.4	10927.96	1.1
	10350.79	1.0	10530.22	0.4	10933.50	1.1
	10372.34	1.0	10558.81	0.4	10977.34	1.1
	10372.43	1.0	10652.12	0.4	10977.70	1.1
dye	17521.00	0.05	17514.27	0.05	17513.80	0.05
	17507.51	0.05	-	-	-	-
Kr^+	17594.91	1.1	-	-	-	-

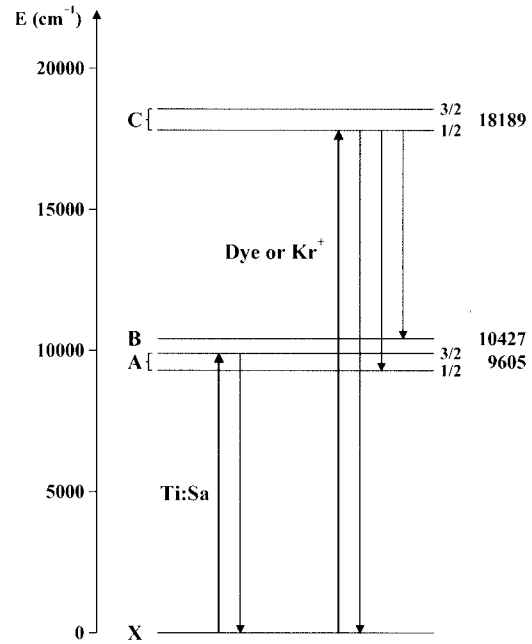

FIG. 2. Energy level scheme of excited and fluorescence-induced transitions.

By using LIF, generated from a Ti:sapphire single-mode laser, and Fourier transform spectroscopy (FTS), Gutterres *et al.* (*1*) assigned more than 2400 observed wavenumbers of the $B^2\Sigma^+$–$X^2\Sigma^+$ band system. The highly congested spectrum of the $B^2\Sigma^+$–$X^2\Sigma^+$ (0, 0) band, obtained from the chemiluminescent reaction Ba + I_2, was also recorded by using FTS. The spectral data set obtained by Leach *et al.* (*2*) was included in a global analysis including both the $B^2\Sigma^+$–$X^2\Sigma^+$ and the $C^2\Pi$–$X^2\Sigma^+$ band systems. A set of 51 molecular constants was calculated and it reproduced both the observed $B^2\Sigma^+$–$X^2\Sigma^+$

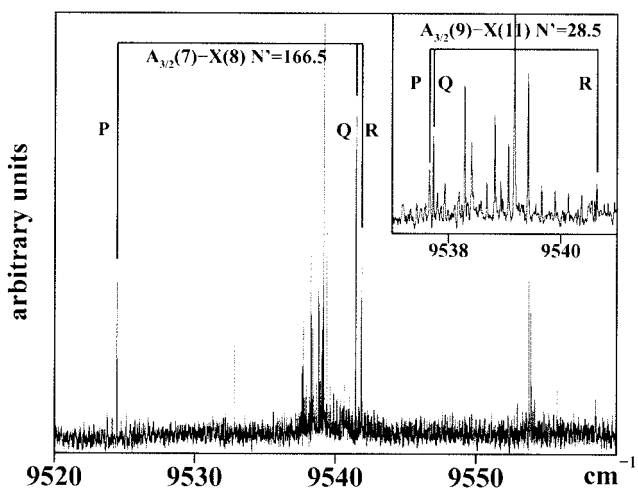

FIG. 3. Part of the *A*–*X* LIF spectrum induced by the Ti:sapphire 10 869.46 cm^{-1} laser line. Numbers in parentheses are the v'' values of the transitions.

TABLE 2

Ti:Sapphire Single-Mode Laser Vacuum Wavenumbers σ, Quantum Numbers v', J', and Energy E' for the $A^2\Pi$ Excited Levels, Quantum Numbers v'', J'', and Energy E'' of the Lower Levels in the Ground $X^2\Sigma^+$ State.

$\sigma(cm^{-1})$	v'	J'	$E'(cm^{-1})$	v''	J''	$E''(cm^{-1})$	Δv
10042.86	2	142.5	10811.27	1	141.5	768.41	1-5
	1	154.5	10756.27	0	154.5	713.40	0-4
	3	79.5	10593.97	2	79.5	551.11	0-6
	2	92.5	10503.84	1	93.5	460.98	0-5
	3	52.5	10648.07	2	52.5	605.21	1-6
10056.79	1	129.5	10587.64	0	129.5	530.85	0-4
	2	52.5	10360.76	1	52.5	303.97	1-5
10100.22	4	254.5	12204.11	2	255.5	2103.89	1-7
	5	282.5	12714.61	3	281.5	2614.39	3-8
	10	89.5	11593.44	8	90.5	1493.22	7-13
	10	134.5	11847.91	8	134.5	1747.69	6-14
	9	149.5	11812.78	8	149.5	1712.56	5-12
10150.27	3	204.5	11499.55	1	204.5	1349.28	1-6
	7	82.5	11014.06	5	81.5	863.79	3-10
	2	254.5	11946.70	0	254.5	1796.43	1-4
	7	40.5	11024.54	5	40.5	874.27	3-10
	7	38.5	11018.19	5	38.5	867.92	3-10
	4	200.5	11890.01	2	200.5	1739.74	1-7
10257.79	8	235.5	12384.91	4	234.5	2127.12	4-10
	10	83.5	11567.16	7	83.5	1309.37	7-13
	10	43.5	11438.17	7	44.5	1180.38	7-13
	10	60.5	11483.16	7	60.5	1225.37	7-13
10350.79	13	149.5	12355.57	9	149.5	2004.78	9-17
10422.82	7	166.5	11686.49	3	166.5	1263.60	3-10
	9	52.5	11324.50	5	52.5	901.61	5-12
	9	29.5	11274.55	5	28.5	851.66	5-12
10422.89	9	52.5	11327.17	5	52.5	904.28	5-12
10436.81	17	145.5	12852.64	12	145.5	2415.83	12-22
	19	64.5	12693.98	14	63.5	2257.17	14-24

Note. Range of observed v values in the $X^2\Sigma^+$ state.

and the $C^2\Pi$–$X^2\Sigma^+$ band systems spectral data, with a standard deviation less than 2.3×10^{-3} cm^{-1}. The several observed transitions with $\Delta v \neq 0$ have permitted the solution to the pure vibrational terms of the Hamiltonian used by Leach *et al.* (*2*) to reproduce the observed transitions.

In this work a spectroscopic study of the $A^2\Pi$ is presented. The $A^2\Pi_{1/2}$–$X^2\Sigma^+$, $C^2\Pi_{1/2}$–$A^2\Pi_{1/2}$, $C^2\Pi_{1/2}$–$B^2\Sigma^+$, and $C^2\Pi_{1/2}$–$X^2\Sigma^+$ band systems were investigated by using LIF and FTS. The spectra of both components of $A^2\Pi$–$X^2\Sigma^+$ (0–0) subband, produced from the chemiluminescent reaction Ba + I_2, were also recorded by using FTS. The near-infrared and visible LIF spectra were obtained from the Ti:sapphire and dye single-mode laser excitations and from a Kr^+ multimode ion laser excitation. Previously recorded data for the $C^2\Pi$–$X^2\Sigma^+$ and $B^2\Sigma^+$–$X^2\Sigma^+$, taken from Gutterres *et al.* (*1*) and Leach *et al.* (*2*), were added to the present work data field. Resolved rotational data, originating from 19 vibrational levels ($0 \leq v \leq 5$ and $7 \leq v \leq 19$) of the $A^2\Pi$ state, 32 vibrational levels ($0 \leq v \leq 31$) of the $X^2\Sigma^+$ state, 24 vibrational levels ($0 \leq v \leq 19$, $21 \leq v \leq 19$ and $v = 26$) of the $B^2\Sigma^+$ state, and 12 vibrational levels ($0 \leq v \leq 4$ and $8 \leq v \leq 14$) of the $C^2\Pi$ state were used in the final analysis. Accurate molecular constants, for the $X^2\Sigma^+$, $B^2\Sigma^+$, $A^2\Pi$, and $C^2\Pi$ states, were derived from a simultaneous treatment of the whole data set.

II. THE EXPERIMENT

The experimental configuration and techniques used were similar to those previously reported (*1*). The production of the

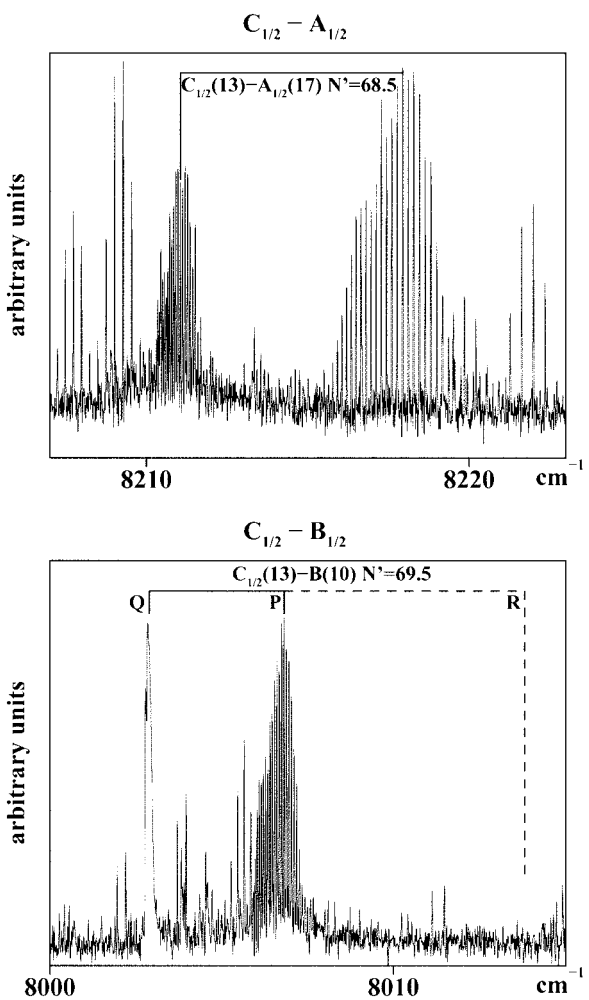

FIG. 4. Part of the *C–A* (on top) and *C–B* (below) LIF spectrum induced by the 17 594.91 cm^{-1} Kr^+ laser line. Numbers in parentheses are the v'' values of the transitions.

TABLE 3

Dye Single-Mode Laser and Kr^+ Multimode Ion Laser Vacuum Wavenumbers σ, Quantum Numbers v', J', and Energy E' for the $C^2\Pi$ Excited Levels, Quantum Numbers v'', J'', and Energy E'' of the Lower Levels in the Ground $X^2\Sigma^+$ State

$\sigma(cm^{-1})$	v'	$\Delta J'$	$\Delta E'(cm^{-1})$	v''	$\Delta J''$	$\Delta E''(cm^{-1})$	Δv^a	Δv^b
17514.27	1	168.5-197.5	18804.48-19085.69	3	169.5-198.5	1290.21-1571.42	0-1	0-2
17521.00	2	165.5-190.5	18924.02-19158.09	4	166.5-191.5	1403.02-1637.09	1-4	1-3
17594.91	9	255.5-256.5	21008.62-21021.78	11	256.5-257.5	3413.71-3426.87	7-13	-
	10	199.5-200.5	20494.15-20504.48	12	200.5-201.5	2899.24-2909.57	8-14	7-8
	10	299.5	21758.02.48	12	298.5	4163.11	-	8
	10	306.5	21865.60.48	12	305.5	4270.69	-	8
	11	133.5-137.5	20061.01-20088.98	13	134.5-138.5	2466.10-2494.07	10-17	8-13
	11	225.5	20920.51	13	224.5	3325.60	-	7
	11	231.5-232.5	20979.05-20990.90	13	230.5-231.5	3384.14-3395.99	-	7-11
	12	62.5-65.5	19848.93-19859.01	14	63.5-66.5	2254.02-2264.10	8-16	9-12
	12	120.5-130.5	20119.21-20183.82	14	119.5-129.5	2524.30-2588.91	8-17	9-14
	13	57.5-77.5	19977.09-20047.69	15	58.5-78.5	2382.18-2452.78	9-18	9-15
	13	203.5-210.5	20961.59-21035.54	15	204.5-211.5	3366.68-3440.63	9-17	9-15
	13	228.5-233.5	21237.95-21296.94	15	229.5-234.5	3643.04-3702.03	9	9-15
	14	130.5-133.5	20469.36-20489.63	16	129.5-132.5	2874.45-2894.72	10-19	11-16

Note. Range of observed v values in the $A^2\Pi$ and $B^2\Sigma^+$ state.
[a] $A^2\Pi$ state.
[b] $B^2\Sigma^+$ state.

BaI molecules was ensured by a heat-pipe oven. This molecular source was proposed by Vidal and Cooper (*19*) and it has been largely used in experimental studies of alkaline–earth monohalides such as BaCl (*20–23*), BaBr (*24*), BaF (*25, 26*), CaF (*27*), and BaI (*1*). In the recording of the LIF spectra a mixture of a few grams of Ba metal and BaI_2 powder was heated to 850°C in the presence of 12 mbar of argon buffer gas. In the chemiluminescent spectrum obtention the same compounds were heated to 1200°C in the presence of 60 mbar of argon buffer gas. The obtained emission in both cases (LIF and chemiluminescent spectra) was focused onto the entrance iris of a 2-m optical path length Fourier transform spectrometer. A scheme of the experimental setup is shown in Fig. 1.

The excitation of the BaI molecules was done using nine laser lines provided by a Ti:sapphire single-mode laser (Coherent 899-21), two laser lines provided by a dye single-mode laser (Coherent 599-21, Rh 6G), and one laser line provided by a Kr^+ (Coherent Innova K 3000) multimode ion laser. The stability of the lasers, in both intensity and frequency, was sufficiently high during the recording time of the spectra (about 2 h). Table 1 shows the spectral characteristics, vacuum wavenumbers, and emitted power of all used laser lines.

The fluorescence spectra were recorded in the region between 9000 and 12 000 cm^{-1} with an unapodized resolution limit ranging from 0.005 to 0.02 cm^{-1}. The wavenumbers were calibrated relative to a fixed frequency reference line (Xe atomic transition near 3.5 μm) used to monitor the path difference of the interferometer. The absolute measurement uncertainty varied from 1×10^{-3} cm^{-1} for the strongest lines to 5×10^{-3} cm^{-1} for the weakest ones.

III. RESULTS

As observed in the spectra of the $B^2\Sigma^+$–$X^2\Sigma^+$ band system (*1*), the recorded spectra presents high complexity. The $A^2\Pi_{3/2}$–$X^2\Sigma^+$, $C^2\Pi_{1/2}$–$A^2\Pi_{1/2}$, $C^2\Pi_{1/2}$–$B^2\Sigma^+$, and $C^2\Pi_{1/2}$–$X^2\Sigma^+$ band systems involve two doublet states; each vibrational band contains several observed rotational branches (six for the $A^2\Pi_{1/2}$–$X^2\Sigma^+$, six for the $C^2\Pi_{1/2}$–$A^2\Pi_{1/2}$, four for the $C^2\Pi_{1/2}$–$B^2\Sigma^+$, and four for the $C^2\Pi_{1/2}$–$X^2\Sigma^+$). In addition, the large mass of barium and iodine atoms results in small rotational constants and consequently the spectra are highly congested. Figure 2 shows an energy level scheme of the involved electronic states in the excitation and the observed fluorescence transitions.

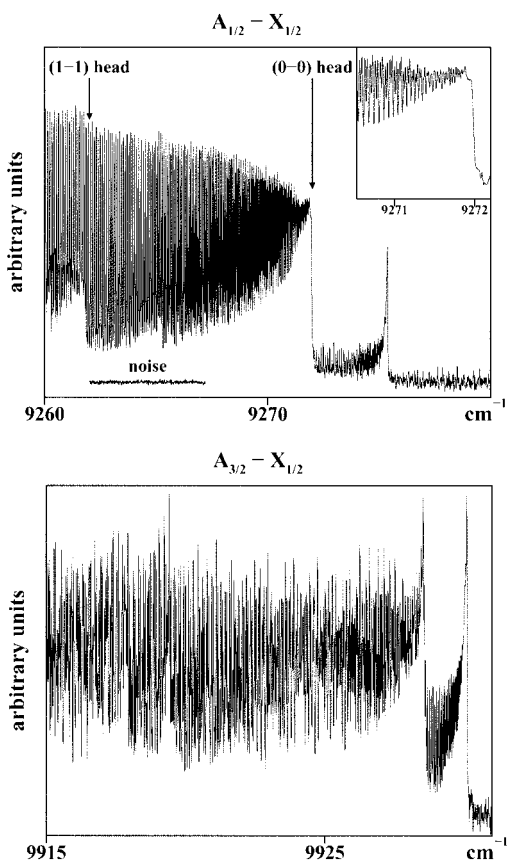

FIG. 5. Part of the chemiluminescent spectrum of the A–X (0, 0) band system for the $A^2\Pi_{1/2}$–$X^2\Sigma^+$ (on top) and $A^2\Pi_{3/2}$–$X^2\Sigma^+$ (below) subbands. The noise level in the spectrum is also depicted.

TABLE 4
Hamiltonian Energy Matrix for the $C^2\Pi$ and $C^2\Pi$ Electronic States

	$^2\Pi_{3/2}$	$^2\Pi_{1/2}$
$^2\Pi_{3/2}$	$T + A/2 + (B + A_J)(X-1)$ $- D[(X-1)^2 + X]$ $+ H[(X-1)^3 + X(3X-1)]$ $+ (A_{JJ}/2)[3(X-1)^2 + X] + (q/2)X$	$- BX^{1/2} + 2DX^{3/2}$ $- HX^{1/2}(3X^2 + X + 1) + A_{JJ}X^{1/2}$ $+ (q/2)[X^{1/2}[-1 \pm (X+1)^{1/2}]]$ $- (p/4)X^{1/2}$
$^2\Pi_{1/2}$	sym.	$T - A/2 + (B + A_J)(X-1)$ $- D[(X+1)^2 + X]$ $+ H[(X+1)^3 + X(3X+1)]$ $- (A_{JJ}/2)[3(X+1)^2 + X]$ $+ (q/2)[X + 2 \mp 2(X+1)^{1/2}]]$ $+ (p/2)[1 \mp (X+1)^{1/2}]$

Note. $X = (J + 1/2)^2 - 1$. Matrix elements are calculated using an e/f parity basis and are written e over f.

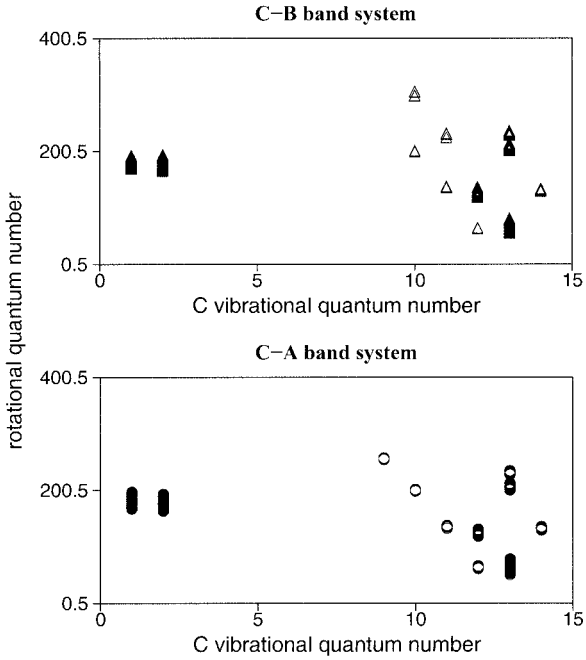

FIG. 6. Schematic representation of the data set used in the reduction of wavenumbers to the molecular constants for the C–B band system (△) and for the C–A band system (○).

A. The LIF Spectra

The LIF technique permits the selection of a small number of coincident laser and molecular line transitions. Consequently the spectra are less congested than those obtained by the classical emission, where a great number of upper excited levels are involved. Therefore the assignment of quantum numbers to the observed transitions is relatively simpler than in the classical case.

1. The $A^2\Pi_{3/2}$–$X^2\Sigma^+$ subband system. Several triplets of P, Q, R lines can be observed in Fig. 3, which shows a part of the recorded LIF spectra of the $A^2\Pi_{3/2}$–$X^2\Sigma^+$ band system. Each line is surrounded by collisional–rotational relaxation lines, their intensities decreasing regularly and rapidly. The intensities of the Q lines are stronger than the intensities of the relative P and R lines, and the six possible branches (P_{21}–Q_{22}–R_{21} and P_{22}–Q_{21}–R_{22}) of this subband system were observed. Much fainter thermal emission appears at the background of the LIF spectrum. This emission is also noted in most parts of the LIF spectra.

Several fluorescence progressions have been observed. Table 2 lists the quantum numbers J', v' and the term energy values E' of the involved $A^2\Pi_{3/2}$ levels together with the quantum numbers J'', v'' and the term energy values E'' of the lower levels in the ground $X^2\Sigma^+$ state. This table also shows the range of observed vibrational levels in the $X^2\Sigma^+$ state. All the line wavenumbers were assigned to transitions involving vibrational levels up to $v' = 19$ in the $A^2\Pi_{3/2}$ state and up to $v'' = 24$ in the $X^2\Sigma^+$ state.

2. The $C^2\Pi_{1/2}$–$A^2\Pi_{1/2}$, $C^2\Pi_{1/2}$–$B^2\Sigma^+$, and $C^2\Pi_{1/2}$–$X^2\Sigma^+$ subband systems. Each laser line of the dye and Kr^+ lasers has excited several and successive rotational levels of the $C^2\Pi_{1/2}$ state and always the vibrational levels of the same state were excited from a $v'' = v' + 2$ vibrational level of the $X^2\Sigma^+$ ground state. Figure 4 shows a part of the recorded LIF spectra of the $C^2\Pi_{1/2}$–$A^2\Pi_{1/2}$ and $C^2\Pi_{1/2}$–$B^2\Sigma^+$ subband systems. Thermal emission relative to the $A^2\Pi_{1/2}$–$X^2\Sigma^+$ and $B^2\Sigma^+$–

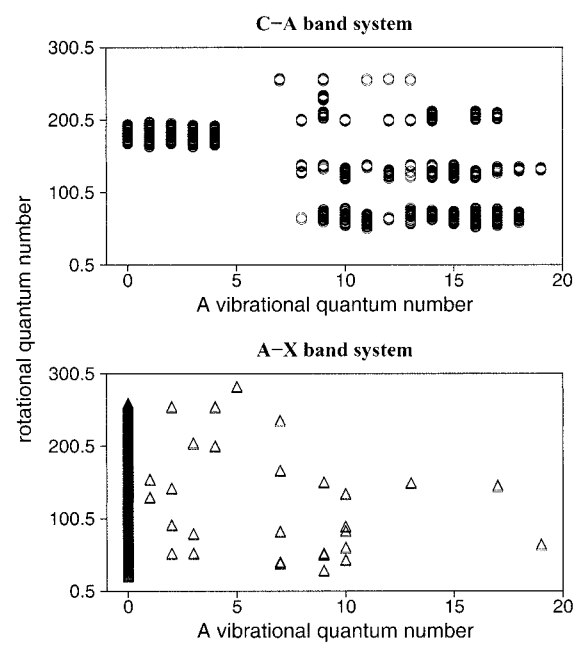

FIG. 7. Schematic representation of the data set used in the reduction of wavenumbers to the molecular constants for the C–A band system (○) and for the A–X band system (△).

TABLE 5

Molecular Constants in cm^{-1} for the $X^2\Sigma^+$ Electronic State Determined in the Analysis from a Nonlinear Least-Squares Fit of the Global Data Set

coeff.	$X^2\Sigma^{+(a)}$	$X^2\Sigma^{+(b)}$	$X^2\Sigma^{+(c)}$
T_e	[0]	[0]	-
$B_e \times 10^{+2}$	2.68040167(704)	2.6805603(479)	2.6805878(8)
$D_e \times 10^{+9}$	3.30413(229)	3.32258(449)	3.3288(10)
$H_e \times 10^{+16}$	-1.932(145)	-1.422(171)	-1.272(80)
$\alpha_B \times 10^{+5}$	6.63379(102)	6.6637046(989)	6.6342(3)
$\beta_B \times 10^{+8}$	3.3739(283)	3.5181(563)	3.397(32)
$\gamma_B \times 10^{+11}$	8.78(156)	6.26(138)	-
$\alpha_D \times 10^{+12}$	1.6117(554)	1.4659(525)	1.31(29)
ω_e	152.163052(101)	152.163530(490)	-
$\omega_e x_e$	0.2726604(221)	0.2726923(204)	-
$\omega_e y_e \times 10^{+4}$	2.36840(546)	2.37572(490)	-
$\gamma_e \times 10^{+3}$	2.53321(192)	2.53721(328)	2.53294(36)
$\gamma_J \times 10^{+10}$	-3.581(173)	-4.051(220)	-3.82(11)
$\gamma_v \times 10^{+5}$	-0.9774(439)	-0.9994(437)	-1.124(11)
$\gamma_{vv} \times 10^{+7}$	-	-1.089(278)	-

Note. Numbers in parentheses represent two standard deviations in units of the last figure quoted.

[a] This work.

[b] Gutterres *et al.* (*1*).

[c] Leach *et al.* (*2*).

$X^2\Sigma^+$ subband systems is also observed in this part of the spectra.

The observed fluorescence progressions are given in Table 3 which summarizes the quantum numbers J', v', and the term energy value E' of the involved $C^2\Pi_{1/2}$ level together with the quantum numbers J'', v'' and the term energy value E'' of the lower level in the ground $X^2\Sigma^+$ state. This table also shows the range of observed vibrational levels in the $A^2\Pi_{1/2}$ and $B^2\Sigma^+$ states. All the line wavenumbers were assigned to transitions involving vibrational levels up to $v' = 14$ in the $C^2\Pi_{1/2}$ state and $v'' = 19$ or 16 in the $A^2\Pi_{1/2}$ or $B^2\Sigma^+$ states, respectively.

B. The Thermal Emission

The spectrum of the $A^2\Pi$–$X^2\Sigma^+$ (0, 0) band, obtained from the chemiluminescent reaction Ba + I_2, is highly congested and the typical separation between the observed lines is lower than 0.01 cm^{-1}. A part of the recorded spectrum can be seen in Fig. 5.

This observed high-spectral density is a consequence of both the similar potential curves of the two states involved in this observed transition (the $A^2\Pi$ and $X^2\Sigma^+$ states) and of the doublet structure of the same states. The separation of the vibrational bands with the same Δv (for low-vibrational levels) is only about 10 cm^{-1} and the overlap in the spectrum of the band systems with the same Δv is severe. In addition, the doublet structure of the involved states has, as a consequence, the splitting of each vibrational band in 12 overlapping rotational branches.

Numerous other bands than the $A^2\Pi$–$X^2\Sigma^+$ (0–0) were observed in the chemiluminescent spectrum. Their small intensities and strong overlaps prevent the inclusion of the corresponding spectral data in the global calculations.

IV. ANALYSIS

The obtained available spectroscopic data of the $A^2\Pi_{3/2}$–$X^2\Sigma^+$, $C^2\Pi_{1/2}$–$A^2\Pi_{1/2}$, and $C^2\Pi_{1/2}$–$B^2\Sigma^+$ band systems, obtained from the LIF spectra and the thermal emission spectrum (0–0 band), were combined with previous results (*1, 2*) and reduced by using a nonlinear least-squares method. Both energy term values of the $B^2\Sigma^+$ and $X^2\Sigma^+$ electronic states were described by standard Hund's case (b) $^2\Sigma^+$ formulae:

$$T = T_v + B_v N(N+1) - D_v[N(N+1)]^2 + H_v[N(N+1)]^3 + \cdots$$

TABLE 6

Molecular Constants in cm^{-1} for the $B^2\Sigma^+$ Electronic State Determined in the Analysis from a Nonlinear Least-Squares Fit of the Global Data Set

coeff.	$B^2\Sigma^{+(a)}$	$B^2\Sigma^{+(b)}$
T_e	10427.02254(52)	10427.02214(43)
$B_e \times 10^{+2}$	2.61129134(792)	2.6114569(480)
$D_e \times 10^{+9}$	3.51124(239)	3.53151(454)
$H_e \times 10^{+16}$	-3.138(148)	-2.510(173)
$\alpha_B \times 10^{+5}$	7.24114(118)	7.24092(131)
$\beta_B \times 10^{+8}$	4.9673(838)	4.8150(592)
$\gamma_B \times 10^{+11}$	12.99(235)	13.56(221)
$\alpha_D \times 10^{+12}$	2.2733(652)	2.4777(913)
$\beta_D \times 10^{+14}$	-	-0.2728(546)
ω_e	141.951364(324)	141.951647(316)
$\omega_e x_e$	0.2896297(272)	0.2748075(534)
$\omega_e y_e \times 10^{+4}$	3.10480(729)	3.10879(674)
$\gamma_e \times 10^{+3}$	-56.41361(371)	-56.40837(416)
$\gamma_J \times 10^{+10}$	116.719(528)	116.816(513)
$\gamma_v \times 10^{+5}$	8.5331(777)	8.4308(763)
$\gamma_{vv} \times 10^{+7}$	-	-1.535(450)

Note. Numbers in parentheses represent two standard deviations in units of the last figure quoted.

[a] This work.

[b] Gutterres *et al.* (*1*).

TABLE 7

Molecular Constants in cm^{-1} for the $A^2\Pi$ and $C^2\Pi$, Electronic States Determined in the Analysis from a Nonlinear Least-Squares Fit of the Global Data Set

coeff.	$A^2\Pi^{(a)}$	$C^2\Pi^{(a)}$	$C^2\Pi^{(b)}$	$C^2\Pi^{(c)}$
T_e	9605.422059(835)	18188.50676(38)	18188.49572(32)	-
$B_e \times 10^{+2}$	2.5946907(842)	2.6726404(207)	2.6727975(489)	2.672800(17)
$D_e \times 10^{+9}$	3.44677(380)	3.04976(271)	3.06861(462)	3.0726(14)
$H_e \times 10^{+16}$	-3.069(201)	-1.722(146)	-1.191(172)	-1.032(80)
$\alpha_B \times 10^{+5}$	7.0507(322)	6.35882(101)	6.362327(968)	6.3610(22)
$\beta_B \times 10^{+8}$	3.5418(459)	2.6955(411)	2.8178(373)	2.50(5)
$\alpha_D \times 10^{+12}$	2.579(117)	1.9218(581)	1.7532(547)	1.693(295)
$\beta_D \times 10^{+14}$	-	-	-	1.06(22)
$A_e \times 10^{-2}$	6.5665872(181)	7.56059855(583)	7.56059476(474)	7.560594(5)
$A_J \times 10^{+6}$	-37.656(101)	-4.0344(163)	-4.0420(133)	-4.0716(108)
$A_{JJ} \times 10^{+12}$	-14.61(227)	4.6740(531)	4.7255(438)	7.253(51)
$A_v \times 10^{+1}$	-5.24916(309)	1.09677(178)	1.09401(148)	1.09045(148)
$A_{vv} \times 10^{+2}$	0.23218(234)	1.6017(124)	1.6482(108)	1.676(11)
$A_{vJ} \times 10^{+7}$	1.5664(775)	3.8074(136)	3.7920(115)	3.8206(107)
ω_e	141.748263(343)	157.795937(395)	157.796220(387)	-
$\omega_e x_e$	0.2754137(426)	0.2748450(523)	0.2748075(534)	-
$\omega_e y_e \times 10^{+4}$	2.4206(141)	2.2177(229)	2.1705(242)	-
$p_e \times 10^{+3}$	-56.2122(447)	7.03502(479)	7.02330(434)	7.0247(39)
$p_J \times 10^{+9}$	20.13(265)	-3.2628(429)	-3.1986(362)	-3.224(31)
$p_v \times 10^{+5}$	6.904(192)	-4.3632(377)	-4.2518(359)	-4.235(40)
$q_e \times 10^{+6}$	25.15(168)	-2.006(394)	-1.885(341)	-1.373(328)
$q_J \times 10^{+12}$	-	12.98(250)	12.53(211)	5.43(398)
$q_v \times 10^{+8}$	321.1(640)	-	-	7.76(183)

Note. Numbers in parentheses represent two standard deviations in units of the last figure quoted.

[a] This work.

[b] Gutterres *et al.* (*1*).

[c] Leach *et al.* (*2*).

$+\frac{1}{2}\gamma N$ for *e*-labeled levels, and $-\frac{1}{2}\gamma(N+1)$ for *f*-labeled levels, with:

$$
\begin{aligned}
T_v &= T_e + \omega_e(v+1/2) - \omega_e x_e(v+1/2)^2 \\
&\quad + \omega_e y_e(v+1/2)^3 + \cdots \\
B_v &= B_e - \alpha_B(v+1/2) + \beta_B(v+1/2)^2 + \cdots \qquad [1] \\
D_v &= D_e + \alpha_D(v+1/2) + \cdots \\
\gamma &= \gamma_e + \gamma_v(v+1/2) + \gamma_D N(N+1) + \cdots .
\end{aligned}
$$

The used Hamiltonian matrix elements for the isolated $C^2\Pi$ and $A^2\Pi$ electronic states are shown in Table 4. The vibrational dependence of the parameters was taken into account by a "Dunham-type" variation. For example,

$$
\begin{aligned}
T_v &= T_e + \omega_e(v+1/2) - \omega_e x_e(v+1/2)^2 \\
&\quad + \omega_e y_e(v+1/2)^3 + \cdots \\
A &= A_e + A_v(v+1/2) + A_{vv}(v+1/2)^2 + \cdots \\
B_v &= B_e - \alpha_B(v+1/2) + \beta_B(v+1/2)^2 + \cdots \qquad [2] \\
D_v &= D_e + \alpha_D(v+1/2) + \cdots \\
p &= p_e + p_v(v+1/2) + p_J J(J+1) + \cdots \\
&\quad + p_{vv}(v+1/2)^2 + \cdots .
\end{aligned}
$$

In the final analysis the $^2\Sigma^+$ electronic states were described in terms of Eq. [1].

Figure 6 shows a schematic diagram of the analyzed vibrational and rotational data field of the *C–B* and *C–A* band systems. The spectroscopic data set obtained in this work, and the one used by the authors of Refs. (*1, 2*) in their final analysis, are complementary. Figure 7 shows the range of the observed *v* and *J* in the $A^2\Pi$ electronic state through the *C–A* and *A–X* band systems.

Tables 5 and 6 summarize the final values of the recommended effective molecular constants for the ground electronic state and for the $B^2\Sigma^+$ electronic state, respectively, derived from the global analysis described above. The values of the molecular constants obtained by Leach *et al.* (*2*) and Gutterres *et al.* (*1*) are quoted in these tables. In the same way, Table 7 summarizes the final values of the recommended effective molecular constants for the $A^2\Pi$ and $C^2\Pi$ electronic states, derived from the global analysis. Also, the values of the molecular constants obtained by Leach *et al.* (*2*) and Gutterres *et al.* (*1*) are quoted in the same table. The standard deviation was less than 2.9×10^{-3} cm^{-1} and a strong similarity between the three sets of obtained molecular constants for the $X^2\Sigma^+$ and $C^2\Pi$ electronic states can be observed.

Table 8 shows the energy origins obtained in this work for the $B^2\Sigma^+$, $A^2\Pi$, and $C^2\Pi$ electronic states, as well as the theoretical values for the same constants derived from the

TABLE 8

Comparison between the Theoretical Values of Transition Energies (in cm^{-1}) and Those Calculated in this Work

State	This work	Allouche *et al.* [6]	Törring *et al.* [3]
$A^2\Pi$	9605.422059(835)	9300	9420
$B^2\Sigma^+$	10427.02254(52)	10003	10160
$C^2\Pi$	18188.50676(38)	21528	21220

Note. Numbers in parentheses represent two standard deviations in units of the last figure quoted.

model of the ligand field approach (*6*) and the electrostatic polarization (*3*). For the $B^2\Sigma^+$ electronic state the difference between the theoretical and the experimental transition energy values is less than 5% for the simpler model of ligand field approach and less than 2% for the model of electrostatic polarization. The difference is however larger than 15% for the two theoretical models in the case of the $C^2\Pi$ electronic state. New calculations are currently in progress for these low excited electronic states of the BaI molecule (*28*). Comments will be reported on the various theoretical methods.

V. CONCLUSION

Laser-induced fluorescence (LIF) and thermal emission, obtained from the chemiluminescent reaction Ba + I_2, combined with Fourier transform spectroscopy (FTS), have permitted the first spectroscopic study with rotational resolution of the $A^2\Pi$ electronic state of the BaI molecule. The data set published in (*2*) and (*1*) for the $C^2\Pi$–$X^2\Sigma^+$ and $B^2\Sigma^+$–$X^2\Sigma^+$ band systems of the BaI molecule was added to the present work data set and a global analysis of $A^2\Pi$–$X^2\Sigma^+$, $B^2\Sigma^+$–$X^2\Sigma^+$, $C^2\Pi$–$X^2\Sigma^+$, $C^2\Pi$–$A^2\Pi$, $C^2\Pi$–$B^2\Sigma^+$ band systems was performed. An improved set of 71 molecular constants was calculated and it described the observed transitions of both band systems with a standard deviation of 2.80×10^{-3} cm^{-1}. In this work the knowledge of the vibrational levels of the $C^2\Pi$ state was extended from $v = 12$ (analyzed by Leach *et al.* (*2*)) up to $v = 14$ (highest observed vibrational level), and the vibrational levels with $v = 9$, 10, 11, and 13, which have not been observed until this moment, could be assigned.

Current work is in progress concerning the $D^2\Sigma^+$ electronic state and the $A'\,^2\Delta$ unobserved electronic state.

ACKNOWLEDGMENTS

This work is partially supported by CAPES/COFECUB (Brazil/France cooperation) 182/96. The authors are grateful to J. Chevillard for skillful help during the recording of the spectra.

REFERENCES

1. R. F. Gutterres, J. Vergès, and C. Amiot, *J. Mol. Spectrosc.* **196,** 29–44 (1999).
2. C. A. Leach, A. A. Tsekouras, and R. N. Zare, *J. Mol. Spectrosc.* **153,** 59–72 (1992).
3. T. Törring, W. E. Ernst, and S. Kindt, *J. Chem. Phys.* **90,** 4927–4932 (1989).
4. T. Törring, W. E. Ernst, and J. Kändler, *J. Chem. Phys.* **81,** 4614–4619 (1984).
5. S. F. Rice, H. Martin, and R. W. Field, *J. Chem. Phys.* **82,** 5023–5034 (1985).
6. A. R. Allouche, G. Wannous, and M. Aubert-Frécon, *Chem. Phys.* **170,** 11–22 (1993).
7. A. R. Allouche, Thèse de Doctorat, Université Claude-Bernard Lyon I, 1993.
8. O. H. Walters and S. Barratt, *Proc. R. Soc. London, Ser. A* **118,** 120–137 (1928).
9. P. Mesnage, *Ann. Phys.* **12,** 5–9 (1939).
10. M. M. Patel and N. R. Shah, *Ind. Appl. Phys.* **8,** 681–682 (1970).
11. M. L. P. Rao, D. V. K. Rao, P. T. Rao, and P. S. Murty, *Fizika* **9,** 25–29 (1977).
12. R. S. Bradford, Jr., C. R. Jones, L. A. Southall, and H. P. Broida, *J. Chem. Phys.* **62,** 2060–2064 (1975).
13. M. A. Johnson, C. R. Webster, and R. N. Zare, *J. Chem. Phys.* **75,** 5575–5577 (1981).
14. M. A. Johnson and R. N. Zare, *J. Chem. Phys.* **82,** 4449–4459 (1985).
15. M. A. Johnson, C. Noda, J. S. McKillop, and R. N. Zare, *Can. J. Phys.* **62,** 1467–1477 (1984).
16. D. Zhao, P. H. Vaccaro, A. A. Tsekouras, C. A. Leach, and R. N. Zare, *J. Mol. Spectrosc.* **148,** 226–242 (1991).
17. C. A. Leach, J. R. Waldeck, C. Noda, J. S. McKillop, and R. N. Zare, *J. Mol. Spectrosc.* **146,** 465–492 (1991).
18. T. Töring and K. Döbl, *Chem. Phys. Lett.* **115,** 328–332 (1985).
19. C. R. Vidal and J. Cooper, *J. Appl. Phys.* **40,** 3370–3374 (1969).
20. C. Amiot and J. Vergès, *Chem. Phys. Lett.* **185,** 310–312 (1991).
21. C. Amiot, M. Hafid, and J. Vergès, *J. Phys. B* **26,** L407–L412 (1993).
22. M. Hafid, C. Amiot, and J. Vergès, *Chem. Phys. Lett.* **210,** 45–49 (1993).
23. C. Amiot, M. Hafid, and J. Vergès, *J. Mol. Spectrosc.* **180,** 121–138 (1996).
24. O. Launila and P. Royen, *Mol. Phys.* **82,** 815–823 (1994).
25. A. Bernard, C. Effantin, E. Andrianavalona, J. Vergès, and R. F. Barrow, *J. Mol. Spectrosc.* **152,** 174–178 (1992).
26. Z. J. Jakubek and R. W. Field, *Phys. Chem. Lett.* **72,** 2167–2170 (1994).
27. C. M. Gittins, N. A. Harris, R. W. Field, J. Vergès, C. Effantin, A. Bernard, J. d'Incan, W. E. Ernst, P. Bündgen, and B. Engels, *J. Mol. Spectrosc.* **161,** 303–311 (1993).
28. S. Raoufi and C. Jungen, unpublished manuscript, 2000.